On the Oscillatory Hydrodynamic Instability of Gravitational Thermal Flows of Liquid Metals in Variable Cross-section Containers

Marcello Lappa[1] and Hermes Ferialdi

[1]Department of Mechanical and Aerospace Engineering, University of Strathclyde, James Weir Building, 75 Montrose Street, Glasgow, G1 1XJ, UK – email: marcello.lappa@strath.ac.uk

Abstract: Natural convective flows of liquid metals in open or closed ducts and containers play a relevant role in a variety of applications in mechanical, materials and nuclear engineering. This analysis follows and integrates the line of inquiry started in past authors' work about the typical properties of these flows and associated hierarchy of bifurcations in rectangular geometries. The Navier Stokes and energy equations are solved in their time-dependent and non-linear formulation to investigate the onset and evolution of oscillatory disturbances and other effects breaking the initially unicellular structure of the flow. It is shown that a kaleidoscope of oscillatory patterns is made possible by the new degree of freedom represented by the opposite inclination of the walls with respect to the horizontal direction. Even minute variations in the geometry and/or initial conditions can cause significant changes. Multiple states exist which can replace each other in given sub-regions of the space of parameters. Observed regimes include: quasi-stationary convection, weakly oscillating rolls, coalescing rolls, traveling waves, and modulated (pulso-traveling) disturbances. Most interestingly, traveling waves can propagate either in the downstream or the upstream direction according to whether the walls are converging or diverging.

Key words: Buoyancy flow, Lateral heating, liquid metals, converging or diverging containers, Instability and bifurcation in Fluid Dynamics.

I. Introduction

Thermogravitational flows of liquid metals are widespread in technology and related engineering applications (Delgado Buscalioni and Crespo del Arco[1]; Kaddeche et al.,[2]; Li et al.,[3]; Okano et al.,[4]; Jaber and Saghir[5]; Lappa[6,7]).

As an example, such flows typically play an important role in the solidification of industrial castings and ingots (Ludwig et al.,[8]; Abhilash et al.,[9]). Similar concepts can be applied to the companion field of "crystal growth from the melt", which is typically concerned with the production of crystals of semiconductor or superconductor materials starting from the corresponding liquid state (Dupret and Van der Bogaert[10]; Monberg[11]).

Additional relevance for such flows lies in the nuclear engineering area. As an example, liquid-metal cooled nuclear reactors (liquid metal fast reactor or LMFR) represent a class of advanced-type nuclear devices where water as the primary coolant has been replaced by a liquid metal (Zrodnikov et al.,[12]). Along the same lines, other applications of a prototypical nature can be found

in heat exchangers for high power electronic devices based on metals (that are liquid at ambient temperature or have a small melting point temperature, see Luo and Liu[13]).

Actual geometries in practice are often found to have shapes with top or bottom boundaries being more or less inclined with respect to the horizontal. In all these circumstances, obviously, a proper knowledge of the circulation pattern established inside the fluid should be regarded as the necessary prerequisite for further developments in these fields. Acquiring the capability to assess in advance the intensity and the patterning behavior of such flows might indeed be the key to implement new strategies aimed either to "product" quality improvement (in typical industrial processes concerned with the solidification of castings and ingots or with the production of high-quality semiconductor crystals for electronic applications) or power-plant optimization (in electronic and nuclear engineering).

Apart from applications of practical or prototypical nature, however, there is no doubt that most of the interest in such subjects is essentially *academic*. Indeed, the instabilities of thermogravitational flows in liquid metals and related hierarchy of bifurcations do exert an appeal to researchers and scientists because of their inherent *complexity*. There seems to be no obvious limit to the richness of such dynamics and the variety of related patterns. Such organized structures (and their spatio-temporal evolution) are often aesthetically pleasing and "philosophically" challenging (in terms of the implications they have on the theory of chaos), which makes them irresistible to theoretical physicists[14].

From a purely mathematical point of view, a rigorous formulation of this problem can be cast in the form of the so-called initial-boundary value problem (IBVP) where the governing balance equations for mass, momentum and energy have to be solved together with the related initial and boundary conditions. In turn, this requires implicitly the adoption of a given solution strategy, be it analytical, approximate (semi-exact) or "numerical".

Determining solutions of the equations governing such flows (Navier-Stokes + energy equations) in analytic form is an extremely challenging task (Ostroumov[15]; Birikh[16]; Lappa[17]). These exact solutions are known to exist only in very special circumstances (most of which being purely "ideal") such as domains infinitely extended along the direction of the imposed temperature gradient or flows attaining a purely "parallel state", that is a kind of motion for which only one of the two velocity components in the plane containing the temperature gradient is not zero (which makes the resulting IBVP problem essentially "linear").

The so-called class of Adomian's Decomposition Methods (see, e.g., Adomian[18], Cherruault and Adomian[19], Babolian et al.,[20]) can provide approximate solutions with no need for linearization, perturbation or discretization. Such approach has been applied with a significant rate of success to the case of liquid metals flowing in converging or diverging channels for a variety of conditions and physical effects (Mankinde[21]; Mhone and Mankinde[22]; Asadullah et al.,[23]). These studies, however, have been limited essentially to unidirectional (Couette-like) flows.

The specific case of thermogravitational flow of liquid metals in differentially heated "converging or diverging" containers, encompassing both a direct (from the hot side to the cold side) and

"return" currents (in the opposite direction), has been addressed most recently by Lappa and Ferialdi[24] on the basis of a hybrid approach relying on the numerical integration of the IBVP problem in conjunction with analytic solutions of the temperature field (used as initial conditions).
Though the main objective of that work was an analysis of the typical structure of the Hadley flow in containers having varying cross-sectional area in the specific case of liquid metals flowing in *steady conditions*, several indications were provided that such a problem may display a much more complex behavior when time-dependence sets in (including a non-trivial dependence on geometrical parameters and the characteristic control parameter, namely, the Rayleigh number, Ra).
The complex (non-monotone) dependence displayed by the intensity of the flow and the related shear stress on the geometry characteristic parameters even in steady conditions and the existence of "inflection points" in the velocity profiles revealed by that study would indeed call for a new analysis specifically conceived to address the potential onset of disturbances of hydrodynamic nature when larger values of the control parameter Ra are considered. The overarching aim of the present study, therefore, is to open up for such inquiry.
Such disturbances are expected to break the typical initial unicellular Hadley flow (Lappa and Ferialdi[24]) via stationary or oscillatory bifurcations and produce significant asymmetries in the problem dependence on the so-called compression (or expansion) ratio (defined as the ratio of the size of the heated wall to that of the cooled wall).

2. Mathematical Model and Numerical Method

2.1 The System

We consider a two-dimensional shallow cavity symmetric with respect to the horizontal direction with average depth d, laterally delimited by solid walls at different temperatures (one cooled, the other heated) having height d_{hot} and d_{cold}. The overall system aspect ratio (A) is naturally defined as its length-to-average-depth ratio A=L/d where $d = (d_{hot} + d_{cold})/2$. Another relevant characteristic geometrical parameter (refer to Fig. 1) is the aforementioned expansion (compression) ratio $\eta=d_{hot}/d_{cold}$, which can be >1 (diverging geometry) or <1 (converging geometry), while for $\eta=1$ one would recover the classical case with horizontal boundaries originally introduced by Hadley[25].
We assume the top and bottom walls to be adiabatic (no heat exchange).
As schematically shown in Fig. 1, the natural buoyancy flow emerging is such configurations for relatively small values of the control parameter consists of a single horizontally elongated convective roll (with fluid rising in proximity to the heated wall, moving along the upper wall from the right side to the left side, moving downward when it meets the left (cold) wall and finally coming back to its original position along the bottom wall).

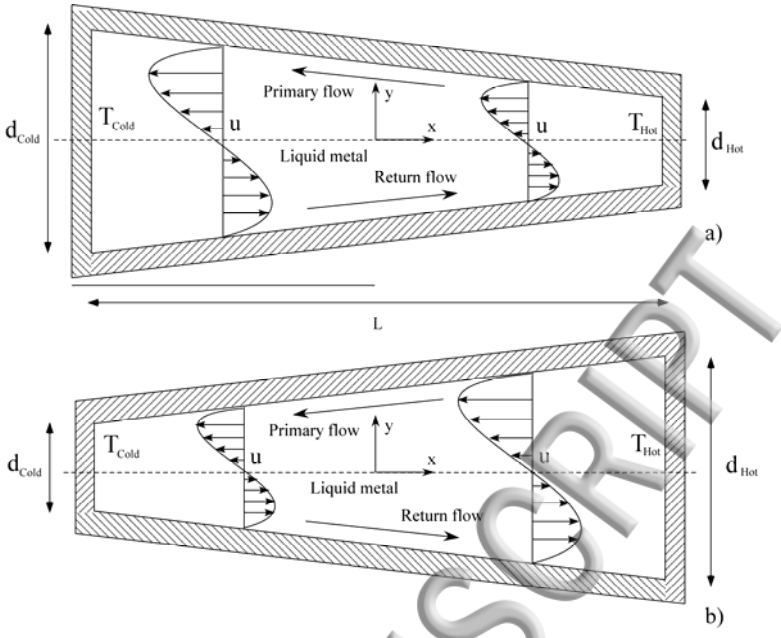

Fig. 1: Sketch of the considered geometry, related thermal and kinematic boundary conditions and reference system: a) $\eta<1$, b) $\eta>1$.

As preliminarily shown by Lappa and Ferialdi[24], both the streamfunction and the nondimensional shear stress being associated with such unicellular flow attain a minimum when the top and bottom walls are perfectly horizontal (the canonical rectangular enclosures which has attracted so much attention in past studies on the subject), i.e. for $\eta=1$. Any departure from this ideal condition, however, can cause an increase in the shear stress and ψ (the related dependence is relatively complex and non-monotone[24]).

These authors also confirmed the presence of "inflection points" in the velocity profile (see again Fig. 1). Such points are known to play a crucial role in determining the "future" behavior of the system when the intensity of the driving force is increased. For purely parallel flow, indeed, it is known that in the case of inviscid dynamics, the following (Rayleigh's) theorem holds: "*In a shear flow a necessary condition for instability is that there must be a point of inflection in the velocity profile* $u=u(y)$*, i.e. a point where* $d^2u/dy^2=0$". As illustrated by Tollmien[26], this theorem can be regarded as also a sufficient condition in many situations (for more comprehensive discussions the interested readers may consider Lin[27], Rosenbluth and Simon[28], Drazin and Howard[29]).

Introducing the fluid Prandtl number as $Pr=\nu/\alpha$ where α is the thermal diffusivity and ν is the kinematic viscosity, such a theorem would be valid in the limit as $Pr\rightarrow 0$. Along these lines, the present study expressly targets an improved understanding of the regimes of fluid motion that are established in converging and diverging geometries in the case of liquid metals (for which $Pr<<1$) when the characteristic control parameter (the Rayleigh number in our case) increases. Here such a parameter is defined as:

$$Ra=GrPr=g\beta_T\Delta T d^3/\nu\alpha \quad (1)$$

where ΔT is the horizontal temperature difference, β_T is the thermal expansion coefficient and Gr=Ra/Pr is the Grashof number.

Given the very small value of Pr considered in the present analysis (Pr=0.01), the simple observations above give rise to the important question to understand whether such flows could become unstable against the onset of disturbances of *hydrodynamic nature* such as those identified in past analyses essentially for parallel flows or convection of liquid metals in rectangular cavities with finite extent (Hurle[30], Hart[31,32], Gill[33], Laure and Roux[34]; Kuo and Korpela[35], Wang and Korpela[36]; Crespo del Arco et al.,[37]; Pulicani et al.,[38]; Okada and Ozoe[39-40]; Gelfgat et al.,[41]). Such instabilities are known to be driven by the mean shear stress (this is the reason why they are often referred to as "shear instability" and the related disturbances as hydrodynamic ones). As a result, a chain of roll is typically created on the frontier of the two opposing (primary and return) horizontal currents characterizing the basic flow. These disturbances are in general stationary (the general outcome of this instability is the replacement of the initial "unicellular" Hadley flow with a multicellular convective structure) and become oscillatory when a second threshold in terms of applied temperature gradient is exceeded[3, 42].

2.2 Governing Equations

Referring velocity and temperature to the scales α/d and ΔT, respectively and scaling all distances on d, the governing equations in nondimensional form (incompressible form) read

$$\underline{\nabla}\cdot\underline{V}=0 \quad (2)$$

$$\frac{\partial \underline{V}}{\partial t}=-\underline{\nabla}p-\underline{\nabla}\cdot\left[\underline{V}\,\underline{V}\right]+\mathrm{Pr}\,\nabla^2\underline{V}-\mathrm{Pr}\,Ra\;T\;\underline{i}_g \quad (3)$$

$$\frac{\partial T}{\partial t}+\underline{\nabla}\cdot\left[\underline{V}T\right]=\nabla^2 T \quad (4)$$

where $\underline{V}$, T and p are the nondimensional velocity, temperature and pressure, respectively, $\underline{i}_g$ is the unit vector along the direction of gravity and the Boussinesq approximation has been used for the buoyancy production term in the momentum equation.

2.3 The Numerical Method, Initial and Boundary Conditions

Though a mathematical basis for the study of these problems is the theory of stability and the theory of bifurcation, however, as shown in different works, also direct numerical discretization and solution of the system model equations (the Navier–Stokes equations in their complete form

This manuscript was accepted by Phys. Fluids. Click here to see the version of record.

together with the energy equation, also referred to as thermal convection equations) can provide significant information.

Here the governing equations have been solved numerically assuming no-slip conditions on the walls, conditions of prescribed temperature at the left and right sidewalls and adiabatic top and bottom (non-horizontal) boundaries.

Moreover, most conveniently (to speed up algorithm convergence), for each simulation the initial temperature field has been initialized using the analytic solution determined by Lappa and Ferialdi[24] in the limit as Ra→0 (diffusive conditions):

$$T(x) = \frac{\ln\left[1 + (\eta - 1)\xi\right]}{\ln(\eta)} \tag{5}$$

where, $\xi = \left(\frac{x}{A} + \frac{1}{2}\right)$ and as shown in Fig. 2, it is to verify that:

$$\lim_{\eta \to 1} \frac{\ln\left[1 + (\eta - 1)\xi\right]}{\ln(\eta)} = \xi \tag{6}$$

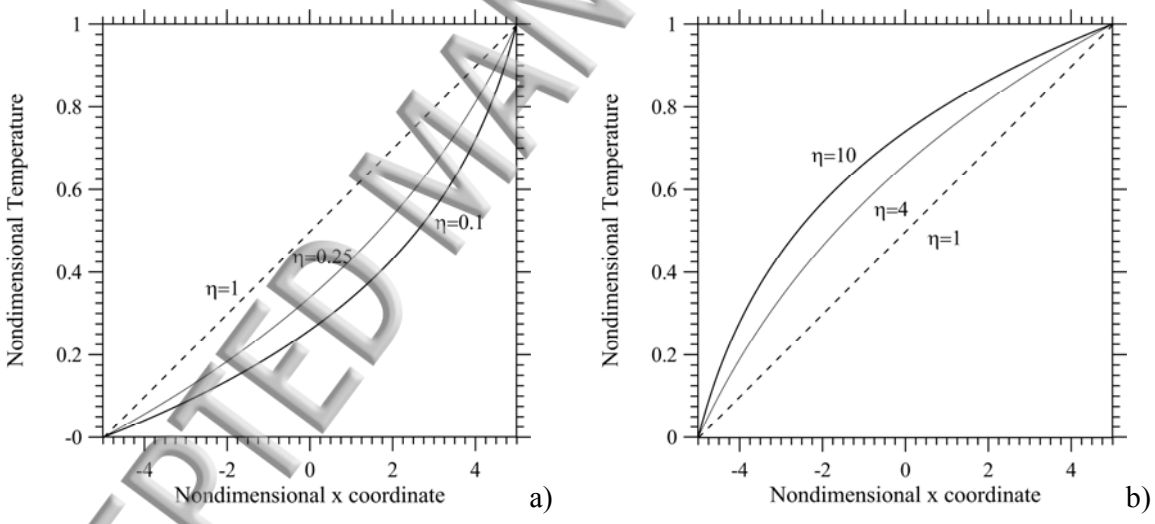

Figs. 2: Exact solution for the temperature distribution plotted for A=10 and Ra=0 (a dashed line is used for the corresponding ideal linear temperature profile): a) η<1 (converging walls); b) η>1 (diverging walls). The temperature profile is concave or convex for η<1 or η>1, respectively.

In particular, we solved the balance equations and related boundary conditions in their complete *non-linear and time-dependent* form using the open source software OpenFoam.

The related solution strategy is based on a classical Finite Volume Method (FVM) approach relying on the spatial discretization of the governing equation cast in integral form over a finite set of control volumes.

This manuscript was accepted by Phys. Fluids. Click here to see the version of record.

With OpenFoam, as for all classical techniques pertaining to the so-called category of projection methods (also known under several other names such as: *fractional-step method or pressure-correction method*, also simply referred to as *primitive-variables approach*), the velocity and pressure fields are treated in a segregated (sequential) manner, with the pressure determined on the basis of a pressure-correction equation obtained using the discrete momentum equation to replace the velocity field in the continuity equation (the so-called PISO approach, the reader being referred to, e.g., Jang et al.,[43] or to the exhaustive book by Moukalled et al.,[44] for additional details).

The implementation of the PISO method in OpenFoam is based on a collocated (non-staggered) variable arrangement for the different problem quantities (which means all primitive variables occupy the same computational points); in order to avoid the emergence of spurious oscillations due to a not well-resolved coupling between pressure and velocity (see, e.g., Choi et al.,[45,46] and references therein), the related solution strategy relies on the well-known Rhie and Chow[47] interpolation stencil. Moreover, both diffusive and convective terms are treated implicitly, whereas other source terms eventually present in the equations (namely the temperature-dependent Boussinesq term in the momentum equation) are treated explicitly.

Because the general problem is formulated and solved in a multistage form, the solution of the energy equation is implemented in the classical segregated way (Patankar and Spalding[48], van Doormaal and Raithby[49]), meaning that the momentum and energy equations are solved one at a time, with the inter-equation coupling treated in an explicit way.

Finally, the pressure (elliptic) equation has been integrated using a standard conjugate gradient method.

2.4 Mesh independence and validation study

The mesh used to solve the problem has been generated using the "blockmesh" utility available in the standard OpenFoam platform. A grid tailoring preliminary analysis for structured grids has been performed towards the end of evaluating (quantitatively) the benefits produced by progressive grid refinement. On the basis of such a study, in particular, we decided to use different meshes according to the aspect ratio (the outcomes of such a preliminary investigation being summarized in Table I).

As shown in Table Ia, for A=4 the minimum mesh required to guarantee independence of the velocity field (and its oscillation frequency) from the used spatial resolution has been found to be 200 points and 50 points along the horizontal and vertical directions, respectively (by doubling the mesh resolution, the change experienced by the disturbance angular frequency is less than 2%).

These results confirm the expectation that, as in the case of liquid metals and moderate values of the Rayleigh number no thermal boundary layers are formed in proximity to the heated and cooled wall, a uniform mesh (fixed space step along the horizontal direction) can adequately capture the dynamic of interest.

For A=10, however, the grid refinement assessment has clearly evidenced the need for a denser mesh. Accordingly, we increased the mesh resolution to 400x50. As shown in Table Ib, for this

This manuscript was accepted by Phys. Fluids. Click here to see the version of record.

value of the aspect ratio and with such a grid, the percentage variations experienced by the angular frequency of the emerging oscillatory disturbances (when the mesh density is doubled) is of the order of 3% even if the worst conditions are considered (η=0.1 and the highest value of Ra examined in the present study).

Table I: Grid Refinement Study: maximum value of the streamfunction or angular frequency ω of measured velocity oscillations as a function of mesh resolution for different values of the aspect ratio A, compression ratio η and Rayleigh number (Pr=0.01).

Table Ia: A=4

η	Ra	parameter	mesh 200x50	mesh 400x100	variation %	Scheme
0.1	5000	ω	1.944	1.906	1.99	Central diff. 2nd order

Table Ib: A=10

η	Ra	parameter	mesh 400x50	mesh 800x100	variation %	Scheme
0.1	9000	ω	0.2666	0.2761	3.04	Central diff. 2nd order

Table Ic: A=4

η	Ra	parameter	mesh 200x50	mesh 400x100	variation %	Scheme
0.5	9000	ψ_{max}	2.717	2.766	1.77	Central diff. (2nd order)
0.5	9000	ψ_{max}	2.772	2.793	0.75	QUICK (3rd order)
0.5	9000	ψ_{max}	2.657	2.741	3.06	Van Leer (2nd order)

The method described in the earlier section was validated through comparison with available results in the literature (Gelfgat et al.,[42]) (see Table II).

Table II: Code Validation Study: Comparison with the results by Gelfgat et al.,[42] for A=4, and Pr=0.015 (present results obtained using a mesh 200x50).

Ra	Angular frequency	value	Code
22170	ω	17.002	Gelfgat et al. (1999).
23000	ω	16.983	Present

This manuscript was accepted by Phys. Fluids. Click here to see the version of record.

As a fundamental part of the general process summarized above, we also deemed it necessary to evaluate separately the role played by the "nature" of the specific numerical "scheme" used to treat the convective terms. Indeed, we could verify that in the delicate process leading a time-marching numerical process to capture a fluid-dynamic instability, the "accuracy" of the scheme (being first order, second order or third order accurate) should not be regarded as an "absolute" parameter or the sole factor determining the success of the used approach.

This is an aspect specifically relevant to the case of hydrodynamic disturbances for which it is generally known that "multiple solutions" can exist for a fixed set of parameters (namely, same geometry and same value of Rayleigh number, Gelfgat et al., [42]). Accordingly, in our research we had to sift through existing studies with different foci in order to get indications and elaborate inferences about what factors may increase the probability of success in such a quest.

It is general consensus that the ability of the algorithm to capture one state or other states depends essentially on the specific initial conditions used for the simulation (Gelfgat, 2017, private communication). This means that different initial conditions should ideally lead to different states (if such alternate states effectively "coexist" in some regions of the space of parameters, Crespo del Arco et al.,[37]; Pulicani et al.,[38]; Okada and Ozoe[39]). As an example in Gelfgat et al.,[42], this philosophy was found to be highly effective in allowing their numerical approach to capture different coexisting solutions starting from different initial conditions.

In the present study we could verify that the emerging hydrodynamic modes can even be sensitive to the specific numerical scheme used to discretize the convective terms in the balance equations. In other words, apart from varying the initial conditions, the use of different schemes can also be instrumental in re-directing the CFD process towards a different state or solution. We will provide some additional information along these lines in Sect. 3 where we discuss in detail the main outcomes of the present work. Here we limit ourselves just to mentioning that this is the reason why Table I about the grid independence analysis contains duplicated data about different cases simulated with three different types of numerical schemes (just to demonstrate our "judicious" use of different computational schemes). As we shall further discuss in Sect. 3, we conducted most of simulations using both central-difference (of the Lax-Wendroff family) schemes and upwind-family schemes (QUICK, Van Leer and related variants, the reader being referred to Moukalled et al.,[44] for the related implementation in OpenFoam). Table Ic clearly proves the intended outcome of such an assessment, i.e. that the ability of the algorithm to converge towards a mesh-independent solution (as the mesh density is increased) is retained when central differences are replaced with the quick or the Van Leer scheme. It also shows that the percentage difference between the results obtained with different schemes lies below 1% even if the worst conditions are considered in terms of Rayleigh number (namely, the highest value of Ra, i.e. 9000).

Though in the majority of cases we found different schemes to give exactly the same results, we could detect *differences in the emerging oscillatory behavior* in a few circumstances. Together with a variation of the initial conditions, such approach allowed us to "detect" effectively the existence of multiples states that is known to be a general feature of this kind of flows.

This manuscript was accepted by Phys. Fluids. Click here to see the version of record.

3. Numerical Results

We concentrate on three specific values of the aspect ratio A, namely A=4 (already extensively considered in past studies on the subject due to its relevance to typical industrial techniques for crystal growth) and A=10 and A=20 to study the system response in the limit as $A\to\infty$ (the case of core flow ideally not disturbed by end walls). Though a discrete set of values for the aspect ratio is selected, however, the corresponding compression (or expansion) ratio is allowed to span a relatively large interval (namely $0.1\leq\eta\leq10$). The system control parameter, i.e. the Rayleigh number is varied in the range $O(10^3)\leq Ra\leq O(10^4)$ with progressive (finite) steps of 1000 in order to assess the evolution of the system from simple steady or weakly oscillatory states up to more complex (multi-frequency and multi-disturbance) situations. By probing the system response for fixed increments in the value of the Rayleigh number, a "grid" of cases is built (and simulated) with the express intention to define a "map" of possible spatio-temporal states in the space of parameters.

3.1 The Zoo of 2D modes

No definition is perfect, and it is hard to distillate a definition from an observation, but the following categorization captures the essential aspects of the phenomena revealed by the present numerical simulations: (i) unicellular steady states (US), (ii) multi-roll steady states (MS), (iii) quasi-stationary states with weakly oscillating rolls (QS), (iv) "classical" oscillatory rolls (with slender "appendages" undergoing a kind of rhythmic displacement) (P), (v) states with periodically touching or "kissing" rolls (K), (vi) regimes with periodically coalescing rolls (C), (vii) purely travelling waves (TW), (viii) mixed states (PLT) with travelling waves "locally" modulated by roll pulsations or splitting behaviors.

Given the complexity of the subject, it is instructive (and "convenient" at the same time) to start from a "canonical case", namely the cavity with perfectly horizontal bottom and top walls. Indeed, this may be regarded as the most natural way to create a link between the present study and valuable earlier efforts in the literature (where the analysis of the nature and structure of hydrodynamic disturbances was limited to the case of purely rectangular cavities).

As already outlined in Sect. 2.4, a notable known feature of these modes is their intrinsic ability to switch from one pattern to another for even minute changes in value of the Rayleigh number or initial conditions. These aspects were originally revealed, e.g., in the landmark studies by Crespo del Arco et al.,[37]; Pulicani et al.,[38]; Okada and Ozoe[39] and Gelfgat et al.,[42], where hydrodynamic modes were found to display a variety of potential behaviors, including the emergence of multi-roll states, transitions from steady to time-periodic solutions, coalescence of multiple states and backward transitions from multi-roll to unicellular regimes. The most interesting of such features was, perhaps, the "multiplicity" of possible solutions, that is, the existence of distinct branches of flow for specific values of the aspect ratio (unlike the bifurcation to transverse-roll flow in the infinite fluid layer, the roll-type structure of convective flow in finite cavities can undergo a

continuous variation of the flow pattern). In general, Gelfgat et al.,[42] found the dependence of the flow on the aspect ratio and the Rayleigh number to be very complex.

3.1.1 Cavity A=4

Without loss of generality, a first example of such dynamics for the present conditions (we consider Pr=0.01) can be seen in Fig. 3, where the pattern emerging from purely diffusive (quiescent) conditions in an enclosure with A=4 and η=1 is shown for two different values of the Rayleigh number:

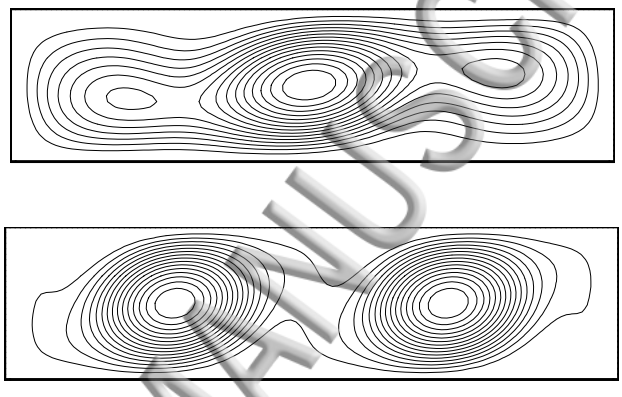

Fig. 3: Multiple steady states of steady convection for A=4 and η=1 (cold and hot sides on the left and on the right of each frame, respectively; upper and lower boundaries with adiabatic conditions): Single- and two-roll steady-state flows for $Ra=1x10^3$ (a), and $Ra=2x10^3$ (b), respectively (two branches of possible steady state exist).

According to our simulations starting from thermally diffusive conditions, for a relatively low Rayleigh number, i.e. $Ra = 10^3$, the flow is simply given by a "twisted" recirculation embracing three co-rotating (anticlockwise in the figures) rolls; when the Rayleigh number is increased, however, a double-vortex configuration also becomes a possible solution of the problem; these flows are both steady and centrally symmetric (namely, the pattern does not change with respect to rotation through 180° about the centre of the cavity).

The patterning behavior as a function of the Rayleigh number can be also tracked by using the synthetic information that we have summarized in Figs. 4. By taking a look at these maps (solutions have been reported there as a function of Ra and arranged accordingly as "columns", whereas "rows" correspond to variations in the value of η), the reader will immediately realize that at η=1 a further increase in the Rayleigh number makes the aforementioned two-roll solution essentially oscillatory (as witnessed by the related finite values of the disturbance angular frequency).

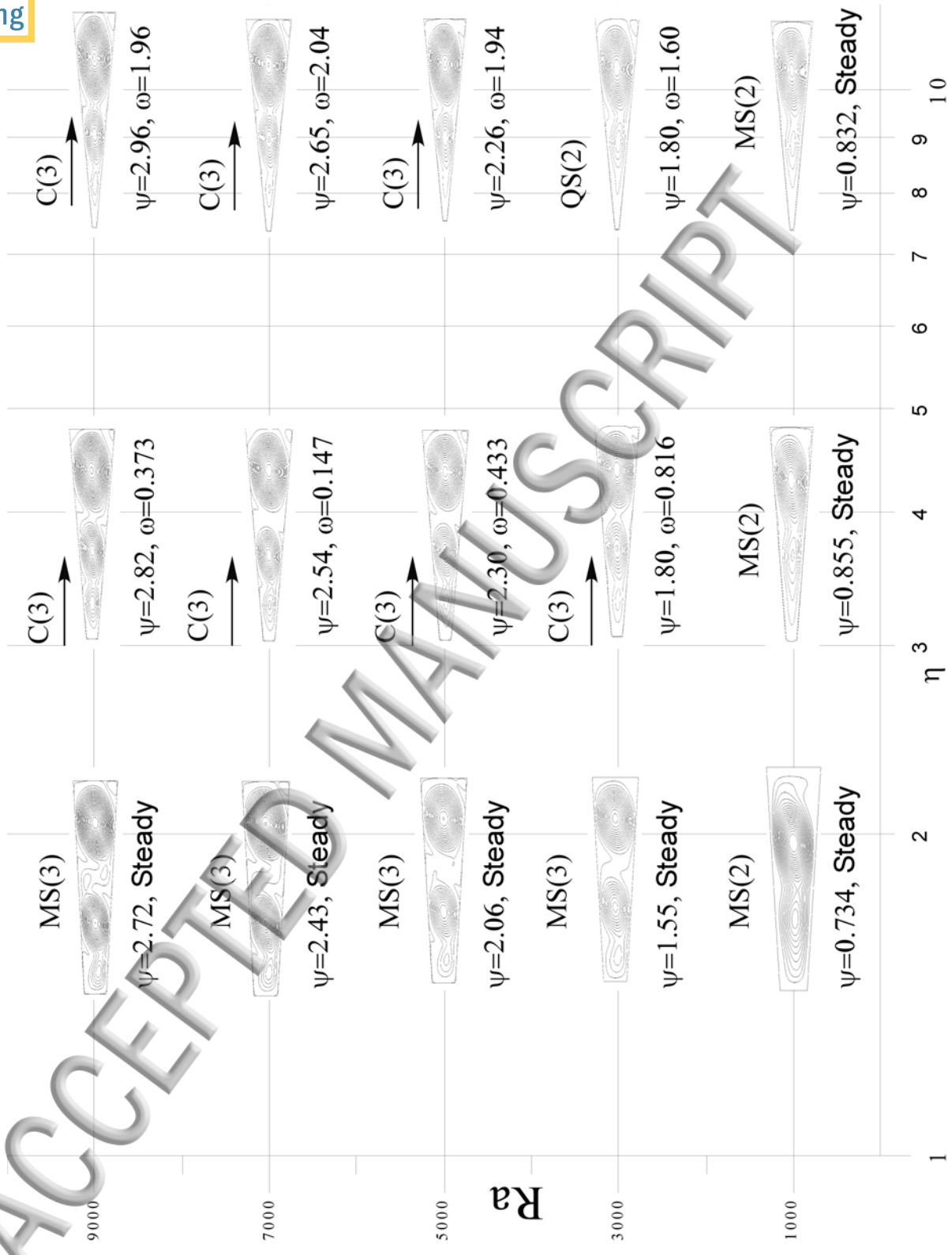

Fig. 4: Map of spatiotemporal states as a function of the parameter η and the Rayleigh number for A=4 (ψ is the maximum of the streamfunction, multiple states existing for a fixed value of η have been reported as separate "columns" at the related value of η and its reverse).

This manuscript was accepted by Phys. Fluids. Click here to see the version of record.

As also reported in earlier numerical studies on this subject for the specific case of rectangular cavities, these oscillatory disturbances appear as morphological variations affecting periodically the shape of the peripheral streamlines of each roll (as shortly mentioned before, the oscillatory distortions may thought of as resembling the rhythmic displacement displayed by the cilia or flagella of bacteria or other microorganisms (P)-mode). A clear example of such a behavior is shown in Fig. 5 for Ra=9000 (multimedia view).

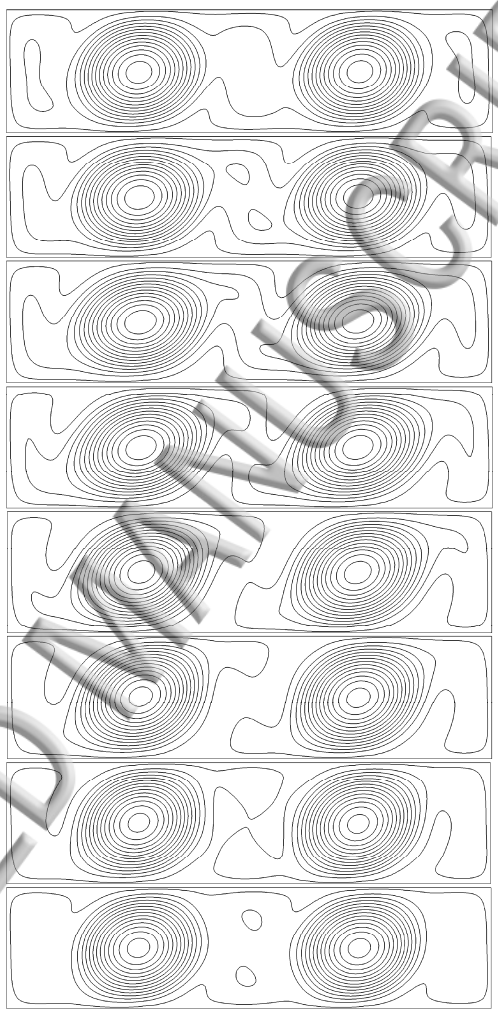

Fig. 5: Oscillatory convection for A=4, η=1 and Ra=9000: eight snapshots evenly distributed during one period of oscillation (multimedia view available).

Additional useful information on such a case can be gathered from Fig. 6. When the threshold for the onset of time-dependence is exceeded (Ra>5000) and the angular frequency of the disturbance increases as a function of the Rayleigh number, the related growth law scales approximately as $(Ra-5.4x10^3)^{1/2}$ (see the P(2) curve in Fig. 6).

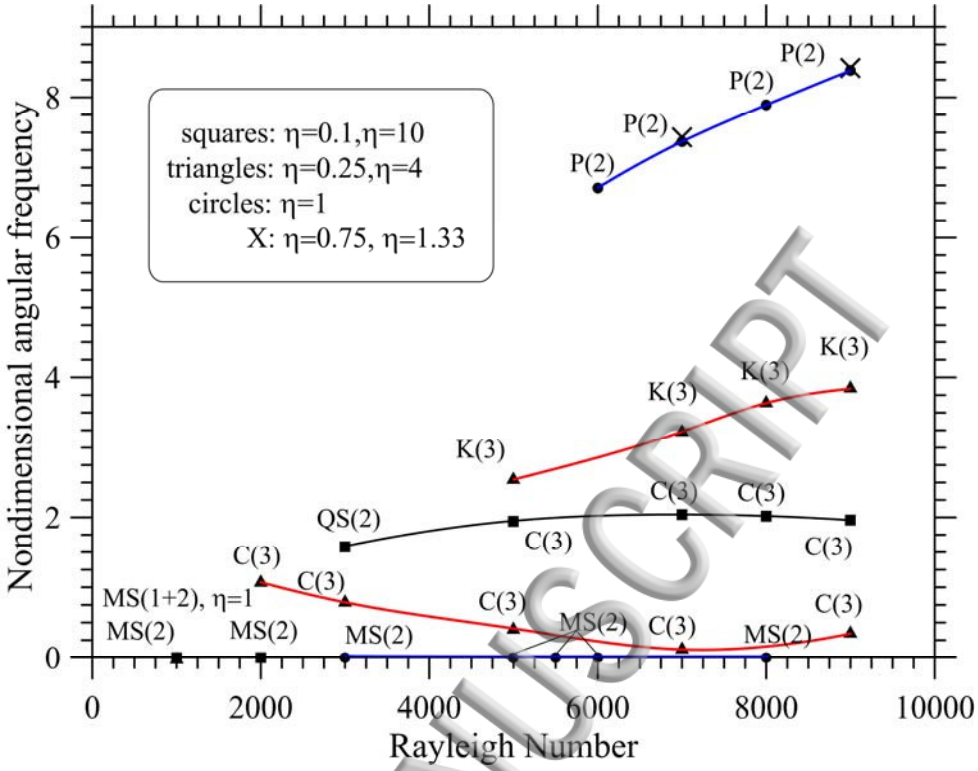

Fig. 6: Oscillatory angular frequency as a function of the Rayleigh number for A=4 and different values of the expansion or compression rate η.

According to the simulations, however, a departure of the expansion (or compression) ratio from the unit value *can produce dramatic changes in the dynamics*, which deserve a separate and exhaustive discussion.

In order to describe such results, conveniently, we start from two representative values of η for which the system behavior is relatively simple, namely the geometry with η=0.5 and the "mirror" configuration with η=2.

As a first distinguishing mark with respect to the case η=1, by taking a look at Fig. 4, the reader will immediately realize that for such cases the flow structure is not center-symmetric. Indeed, this kind of symmetry is no longer a property of the physical domain and, as a natural consequence, it cannot be inherited by the related pattern. The most striking finding emerging from the analysis of these cases, however, is the strong stabilization experienced by convection in the considered range of Rayleigh numbers (the P(2) branch visible in Fig. 4 for η=1 is taken over by a branch of steady states for η=0.5) .

Though no onset of oscillations occurs for the range of Rayleigh numbers visible in Fig. 4, however, some interesting phenomena when the driving force is increased can still be observed: the initial flow with two rolls (m=2) visible for Ra=1000 (similar to that seen in Fig. 3b) is taken over by a three-roll structure when the Rayleigh number is increased to Ra=2000. This new state seems to be rather stable, as we could not detect any change in the number of rolls (or transition to oscillatory

state) for Ra up to 16000 (we had to increase Ra to 16.500 in order to find P(2) oscillatory flow, with an angular frequency 8.82).

Most notably, the behavior observed for η=0.5 is the "mirror image" of that for η=2. In facts, as shown in Fig. 4, the related patterns are "identical" in terms of number of rolls and related morphological properties: as an example, all the flow configurations for η=0.5 could formally be turned into those obtained for the same value of the Rayleigh number for η=2 by simply applying a rotation of 180°. By replacing the hot side with the cold side, indeed such a rotation turns the initial problem with η<1 and gravity directed downwards (where the fluid raises in proximity to the sidewall of smaller size, namely the hot wall located on the right of the figure) into a completely equivalent problem for η>1 in which gravity is directed upwards and the fluid raises in proximity to the cold side (the cold side being located on the right side after the 180° rotation). Hereafter, we will refer to this property of the velocity field for η≠1 as the "*180°-rotation invariance principle after η reversal*", which from a purely mathematical point of view would be equivalent to the following transformation (the tilde being used to indicate the transformed quantities):

$$\begin{bmatrix} \tilde{u} \\ \tilde{v} \end{bmatrix}_{\eta} = \underline{\underline{R}}(180°) \begin{bmatrix} u \\ v \end{bmatrix}_{1/\eta} \quad \text{with the rotation matrix defined as} \quad \underline{\underline{R}}(\theta) = \begin{bmatrix} \cos\theta & -\sin\theta \\ -\sin\theta & \cos\theta \end{bmatrix} \tag{7}$$

Notably, however, the same transformation would *not* work for the temperature field, i.e.

$$T(\tilde{x}, \tilde{y})_{\eta} \neq T(x, y)_{1/\eta} \tag{8}$$

(we will explore other theoretical extensions which attach to the above arguments later in this work).

We observed the response of the system to be similar to that just described for η=0.5 and η=2 in a given neighborhood of these values of η (the system experiencing strong stabilization for 0.4≤η<0.75 and 1.33<η≤2.5). As shown in Fig. 4, however, for η=0.75 (η=1.33) oscillations of the P type are again possible for Ra≥7000. This behavior also occurs at η=0.65 (η≅1.5) provided the Rayleigh number is increased to Ra≥9000.

Nevertheless, further departure of η from these conditions (i.e. η smaller than 0.4 or larger than 2.5) makes the flow again sensitive to the onset and amplification of oscillatory disturbances for *moderate values* of the Rayleigh number. This can be seen again in Fig. 4: for both η<0.4 or η>2.5 we identified transition to time dependence for relatively small values of Ra (the corresponding angular frequency values can be found directly in this figure; hereafter, we will limit ourselves just to discussing the results for η<1, those for η>1 being related to the former by the abovementioned invariance principle).

As an example, in a limited neighborhood of η=0.25 (0.2≤η≤0.3), initially steady flows with m=2 for Ra=1000 are quickly taken over by oscillatory states for Ra≥2000.

The related frequencies are generally smaller than those pertaining to states of the P type (see again Fig. 6). An interpretation of these cases, however, is not as straightforward as one would imagine.

This manuscript was accepted by Phys. Fluids. Click here to see the version of record.

Indeed, in this range of η, we found the variation of angular frequency with Ra (shown in Fig. 6, e.g., for η=0.25) to follow a non-trivial path potentially hiding different mechanisms.

Keeping fixed the initial conditions (corresponding to quiescent and thermally diffusive conditions as explained in Sect. 2.3) and the numerical scheme used for the treatment of the convective terms (central differences) as we did for the solutions shown in Fig. 3, we noticed for $0.2 \leq \eta \leq 0.3$ sudden changes in the typical spatio-temporal behavior displayed by the emerging solutions at different values of the Rayleigh number, which might the typical "signature" of multiple states coexisting in the considered sub-region of the space of parameters.

The "non-progressive" nature of these modes of convection in the space of parameters (the solution jumping from one regime to another in an apparently illogical way when changing the Rayleigh number or η) led us to address the question of understanding whether such apparent "discontinuities" in the system response might be a consequence of the well-known property of the Hadley flow in liquid metals to support multiple states of convection.

In this range of values of η ($0.2 \leq \eta \leq 0.3$) and for $Ra \geq 3000$ we identified two different kinds of solutions alternating in the space of parameters, namely states pertaining to the (K) or (C) regime.

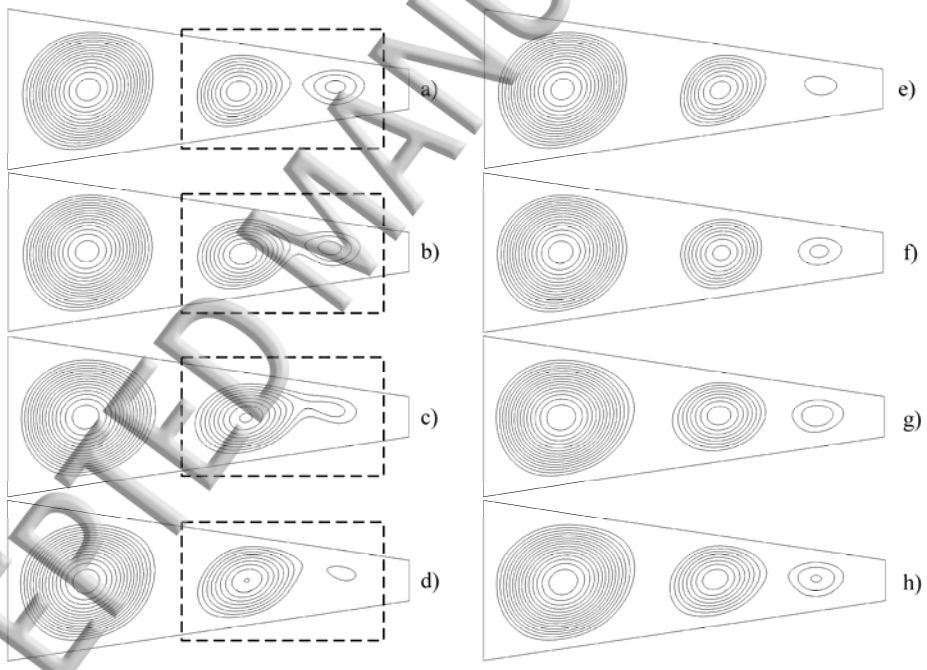

Fig. 7: Oscillatory convection of the (K) type for A=4, η=0.25 and Ra=9000: eight snapshots evenly distributed during one period of oscillation (multimedia view available).

Examples of such states are shown in Figs. 7 and 8 (multimedia view). Though for both cases, the related flow is characterized by the presence of three rolls, the typical features displayed by the emerging oscillatory flow, however, are rather different. In the following, in particular, first we describe the (K) states (which have been occasionally observed also in past studies dealing with

classical rectangular cavities), and then concentrate on the (C) regime, which seems to be specific of geometries with $\eta \neq 1$.

In the first case, two of the tree rolls present at the same time in the cavity (the roll in the center and the roll located in proximity to the right wall) undergo a weakly oscillatory process in which one roll touches periodically its neighbor ("kissing" rolls behavior, which explains why we used a "K" letter to label it). As shown, e.g., by the simulations for $\eta=0.25$ and $Ra=9000$, when the two rolls meet, a single circulation (encapsulating the two initially distinct rolls) is temporarily established in the right part of the cavity (while a single roll remains steadily located in proximity to the left (cold) wall).

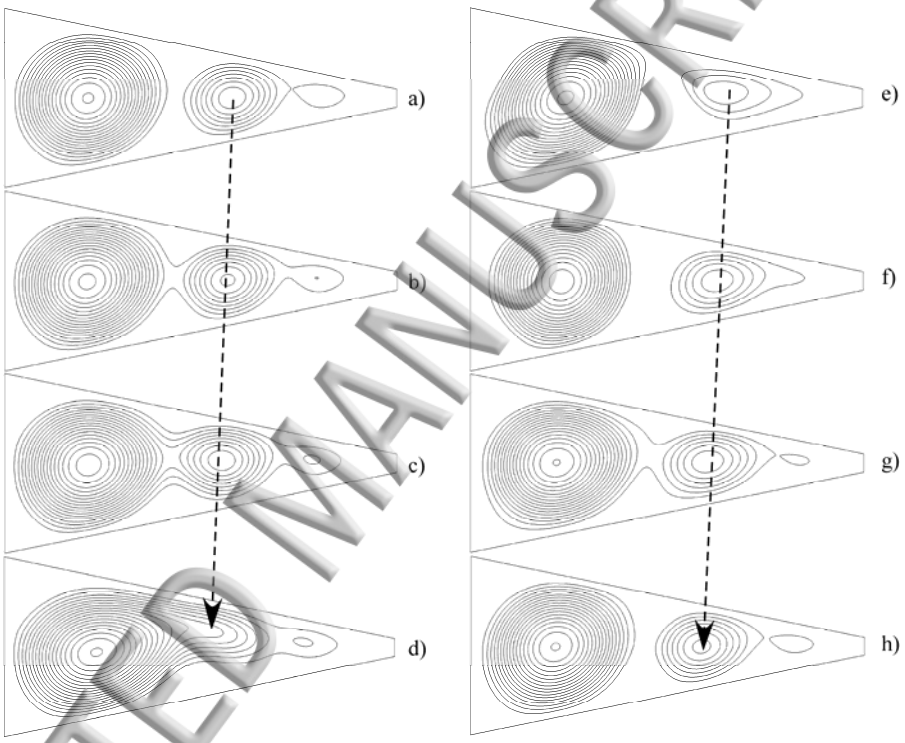

Fig. 8: Oscillatory convection of the (C) type for A=4, $\eta=0.1$ and Ra=9000: eight snapshots evenly distributed during one period of oscillation (multimedia view available).

When solutions pertaining to the (C) regime emerge, however, the spatio-temporal behavior is completely different. According to the simulations, indeed, the above dynamics with the two (central and right) distinct periodically touching rolls are replaced by a much more evident coalescence phenomenon. This process takes place essentially in the left part of the cavity as a result of the displacement of the roll initially located in the center of the cavity towards the left.

When the central and left rolls merge completely, a new roll nucleates on the right side thereby making the entire process an *endless phenomenon* (remarkably, this also gives the observer the feeling of a *disturbance continuously spreading from the right side to the left side*, i.e. in a direction opposite to the temperature gradient). We could observe exactly the same mechanisms for $\eta \geq 3.3$.

This manuscript was accepted by Phys. Fluids. Click here to see the version of record.

However, in this range of η we found the disturbance to propagate from the left side to the right side, i.e. in the same direction of the applied temperature difference (we will come back to this apparently innocuous observation later).

We observed this alternate mode of convection (with a disturbance spreading from regions of reduced cross-sectional area towards regions where the area is larger) to become *the preferred mode of oscillatory instability* in the end regions of the considered interval of η (namely when η is very small or very large, see, e.g., Fig. 8 for η=0.1). As a clear distinguishing mark of this waveform with respect to the (K) regime we also found its frequency to display a relatively weak dependence on the Rayleigh number (the reader being referred again to Fig. 6).

As mentioned before, we identified both modes of convection ((K) and (C)) to be present in the range 0.2≤η≤0.3 (delimited by the vertical dashed lines in Fig. 9) with no apparent progression or connection between the two states (this leading to an apparently scattered set of frequency points in this interval).

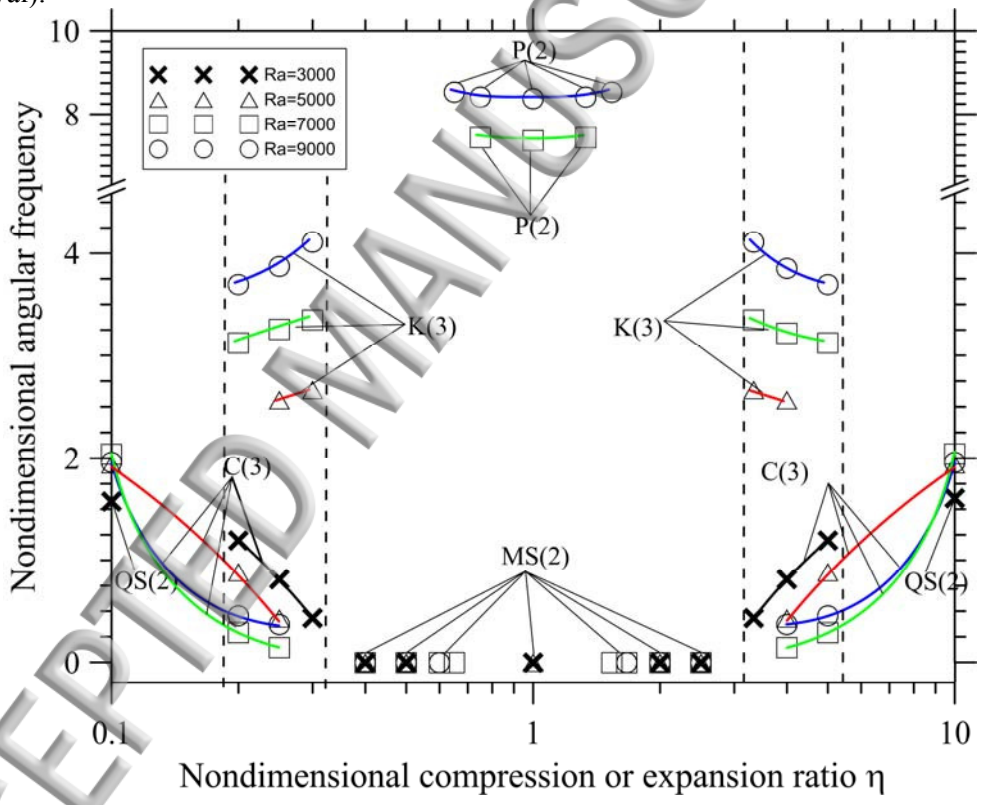

Fig. 9: Oscillatory angular frequency as a function of the expansion or compression rate η for A=4 and different values of the Rayleigh number.

Though this counterintuitive behavior initially resisted our attempts to clarify the underlying dynamics (due to its disorganized appearance in the space of parameters), the strategy discussed in Sect. 2.4 was instrumental in leading us to the conclusion that these two modes of convection are both possible solutions to the problem. In order to do so we performed several numerical simulations for fixed couples (η, Ra) by changing the initial conditions (i.e. starting from a uniform

temperature distribution or using the solution obtained at a given value of the Rayleigh number as initial condition for other values of Ra) and/or applying the other "principle" defined in Sect. 2.4, namely the use of a different category of schemes for the convective term in the energy and momentum equations. As an example, by replacing the central difference scheme with a scheme of the upwind family (the Van Leer) we successfully observed the (K) states found for η=0.25 to turn into spatially spreading (C) modes.

This peculiar approach was instrumental in turning our initial conjecture about the existence of multiple states of convection into reality. Among other things, it also allowed us to "reconstruct" the clearly recognizable continuous different branches reported in Fig. 6 for η=0.25.

Some additional illuminating insights into the above scenario can be obtained by taking a look at the ensemble picture provided by Fig. 9 where the angular frequency has been reported as a function of the parameter η for different (fixed) values of the Rayleigh number.

This figure clearly shows the existence of multiple solutions with their different frequency and convective modes in selected sub-intervals of η (delimited by vertical dashed lines in this figure); outside these intervals, the just discussed strategy based on the use of different initial conditions and spatial integration schemes did not produce any notable change in the emerging solutions.

Leaving aside for a while the existence of multiple states and their influence on the considered problem, other remarkable or notable features of this plot can be summarized as follows: it makes particularly evident the difference in the dynamics occurring in a given neighborhood of η=1 and those occurring in the two external regions ($\eta \leq 0.3$ and $\eta \geq 1.33$). In such regions time-dependence sets in for much smaller values of the Rayleigh number; moreover, for a fixed value of Ra the frequencies are relatively smaller than those obtained in the inner region. Superimposed on such observations is the fact that while for η in the central region the dynamics are rather similar to those already known for rectangular cavities, in the two "external" right and left intervals some heretofore unseen mechanisms become possible (i.e. the (C) mode with the spatially spreading disturbance).

The regions supporting different spatio-temporal behaviors are separated by conditions of stable flow (for $0.3<\eta<0.65$, $1.5<\eta<3.33$ and $Ra<7000$), which further support the idea that a substantial change occurs in the fundamental mechanisms driving oscillatory flow when such bounds are crossed. While in the internal region modes of the P type seem to be the preferential mechanism of oscillatory flow, the external regions are dominated by (C) modes (though (K) solutions are possible as well in some intervals). As shown in Fig. 9, the region of existence of (P) modes increases with Ra. Vice versa the size of the η intervals in which (C) disturbances are possible seems to expand when Ra becomes smaller (we will come back to this interesting finding in Sect. 3.1.2).

As a concluding remark for this section, we limit ourselves to mentioning that at the highest values of the Rayleigh number considered (namely $Ra \geq 7000$) we could find in some cases (η=0.2 and η=5) modes of the (K) and (C) type *to coexist* in the same numerical solutions (mixed states), as witnesses by the presence of two distinct frequencies clearly recognizable in the frequency spectrum for such cases.

Fig. 10: Map of spatiotemporal states as a function of the parameter η and the Rayleigh number for A=10 (ψ is the maximum of the streamfunction, multiple states existing for a fixed value of η have been reported as separate "columns" at the related value of η and its reverse).

3.1.2 Cavity A=10

This section is devoted to examining another important aspect embedded in the considered problem, namely, its dependence on the aspect ratio.

By concentrating on a relatively high value of the aspect ratio (that is A=10), we could obtain some additional interesting insights into the properties of the emerging convective modes, especially for the case of spatially travelling disturbances. Indeed, we found such a perturbation to become the dominant (or preferential) mode of oscillatory convection through the entire range of Rayleigh numbers and values of $\eta \neq 1$ considered, with some interesting "variants" or mixed states emerging for specific couples (η, Ra). Along these lines, in the present section we change completely approach with respect Sect. 3.1.1 and expressly initiate the description of the observed dynamics from the ends of the interval of η rather than from its center.

The related evolution as a function of Ra can be gathered from Fig. 10 and Fig. 11 (these figures give information on the patterning behavior and frequency dependence on Ra, respectively).

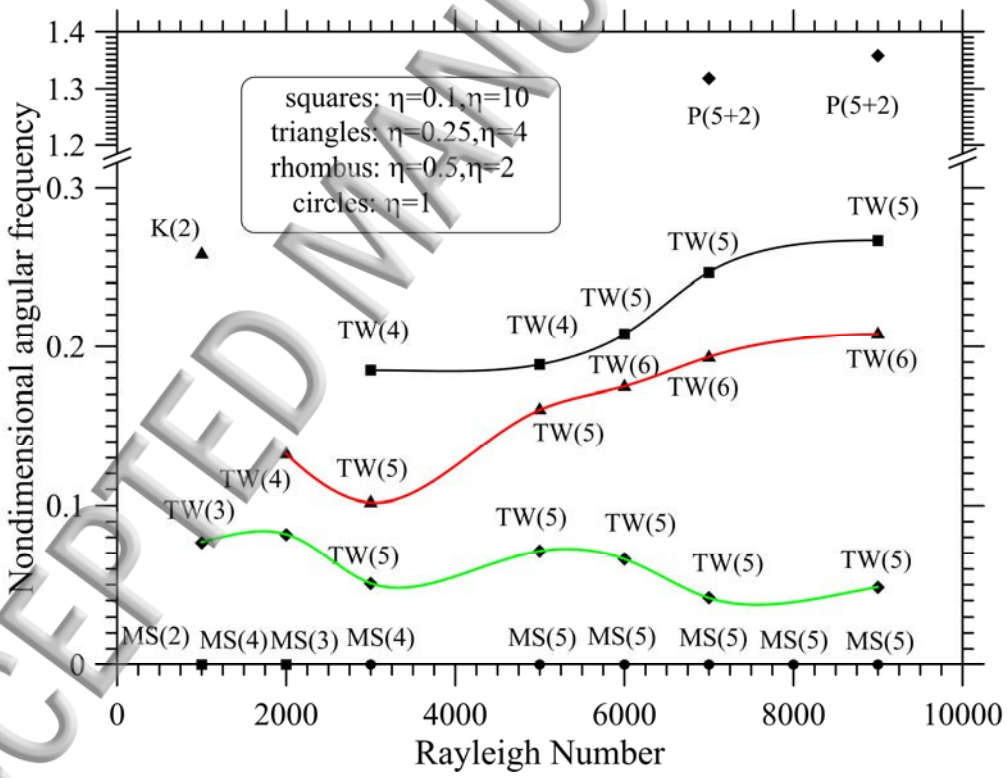

Fig. 11: Oscillatory angular frequency as a function of the Rayleigh number for A=10 and different values of the expansion or compression rate η.

It is worth starting the related description from the simple observation that, for both η=0.1 and η=10, the initially steady solution obtained for Ra=1000 and 2000 is quickly taken over by an oscillatory mode of convection for higher values of Ra. A remarkable feature of this emerging mode

This manuscript was accepted by Phys. Fluids. Click here to see the version of record.

is that the disturbance always clearly travels in the direction in which the cross-section of the domain increases, namely from the hot wall to the cold wall for converging walls and in the *opposite direction* in the case of diverging walls. In practice, the oscillatory disturbance manifests itself as a well-defined series of cells moving from the side with smaller vertical extension towards the other side (Fig. 12, multimedia view).

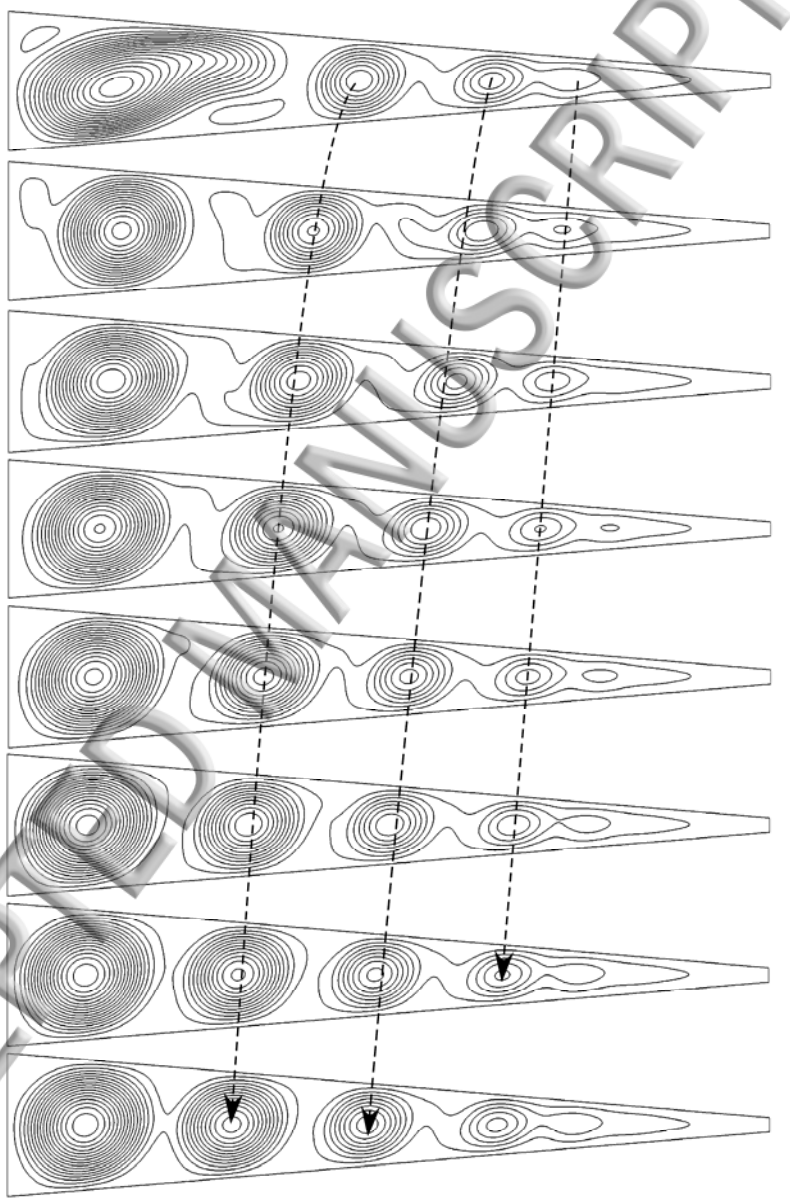

Fig. 12: Oscillatory convection for A=10, η=0.1 and Ra=9000: eight snapshots evenly distributed during one period of oscillation (multimedia view available).

Interestingly, however, an almost motionless roll remains steadily located in proximity to the target wall, regardless of whether η<1 or η>1 (in practice, such a stationary roll is maintained in that

location by the relatively strong buoyancy forces being active in the portion of the domain with larger vertical extension).

When one of the moving cells meets this roll, a coalescence mechanism is triggered (leading to the incorporation of the incoming smaller cell into the larger roll). When the coalescence process is finally over, a new roll nucleates in proximity to the other sidewall, thereby *preserving the average number m of convective cells present in the cavity at any instant* (and making the overall process cyclic).

We clearly detected such dynamics at all the considered values of $Ra \geq 3000$ for both $\eta=0.1$ and 10, which could (with no doubt) be regarded as the clear manifestation of "waves" (TWs) travelling in the system, such a conclusion being also supported by the velocity signals provided by N "numerical probes" evenly distributed along the horizontal direction. The typical signature of a disturbance travelling continuously along a given direction, indeed, is represented by a continuous phase shift visible in the signals measured at different locations, which are equally spaced along the direction of propagation (Fig. 13).

An exception to the above scenario is obviously represented by the aforementioned roll coalescence process occurring in proximity to the sidewall with larger vertical extension (the cold wall for $\eta=0.1$, the hot wall for $\eta=10$). Along these lines, Fig. 13 reveals that the velocity of propagation of the wave is not constant along the x axis. The train of moving rolls targeting the sidewall can be clearly seen to accelerate in the course of their migration (see also Fig. 12). For $\eta<1$, in the left side of the cavity (say $x<A/2$) the velocity of the rolls increases until the first roll of the chain "meets" the vortex residing in proximity to the sidewall. At that stage the two rolls merge and a new roll nucleates in proximity to the other sidewall (the right side for $\eta<1$).

A general picture of the overall scenario can, therefore, be provided as follows: for $\eta<1$ the group of cells spatially spreading periodically towards the side with larger vertical extension (the left side) is bounded from the right (where such rolls are being continuously created) by the hot wall and from the left (where their propagation velocity rises) by a region where coalescence (C) periodically occurs between an incoming roll and another roll being steadily located there (such a localized roll coalescence phenomenon is responsible for the additional high-frequency pulsation mechanism evident in the velocity signal at the station "2" in Fig. 13).

The clearly traveling nature of the disturbance is relatively surprising if one takes into account that transverse waves have never been observed or predicted for the case of laterally heated liquid metals. This behavior becomes even more evident when the A=20 case is considered (Fig. 14, multimedia view).

The intrinsic properties of the TW (its direction of propagation parallel to the horizontal direction with travelling rolls having axes perpendicular to the basic flow) support the conclusion that such a phenomenon is still of a hydrodynamic kind, as the so-called "helical waves" of hydrothermal nature (which are also known to potentially affect gravitationally unstable liquid metals), generally travel in the spanwise direction, i.e. perpendicularly to the basic flow (the interested reader being

referred to Hart[31,32]; Gill[33]; Laure and Roux[34] and Kuo and Korpela[35] for additional information on this mode of convection).

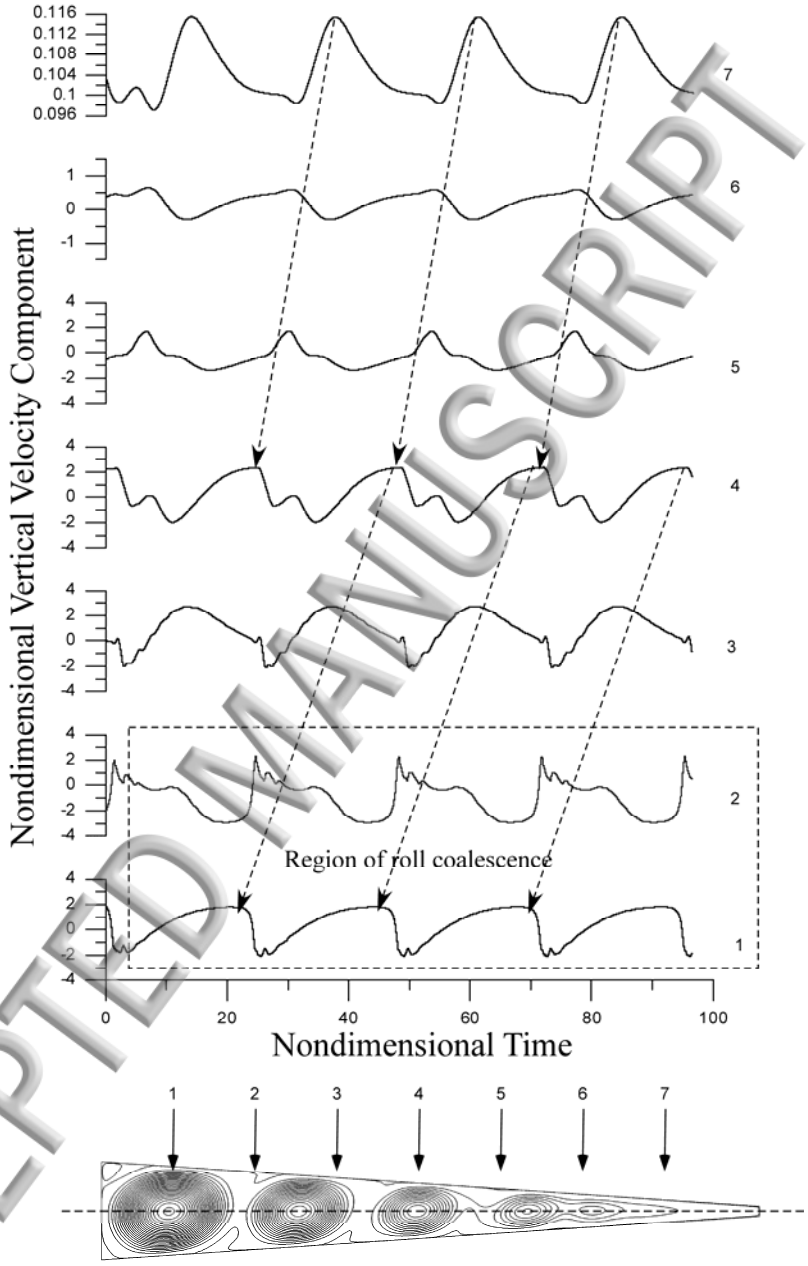

Fig. 13: Velocity signals provided by six probes equally spaced along the horizontal direction (A=10, η=0.1 and Ra=9000, vertical velocity component measured at y=0). The modulation of the sinusoidal signals being related to the main frequency is due to the presence of a second multiple frequency for this relatively value of the Rayleigh number. The irregular behavior displayed by the probe 2 is due to the vortex coalescence process.

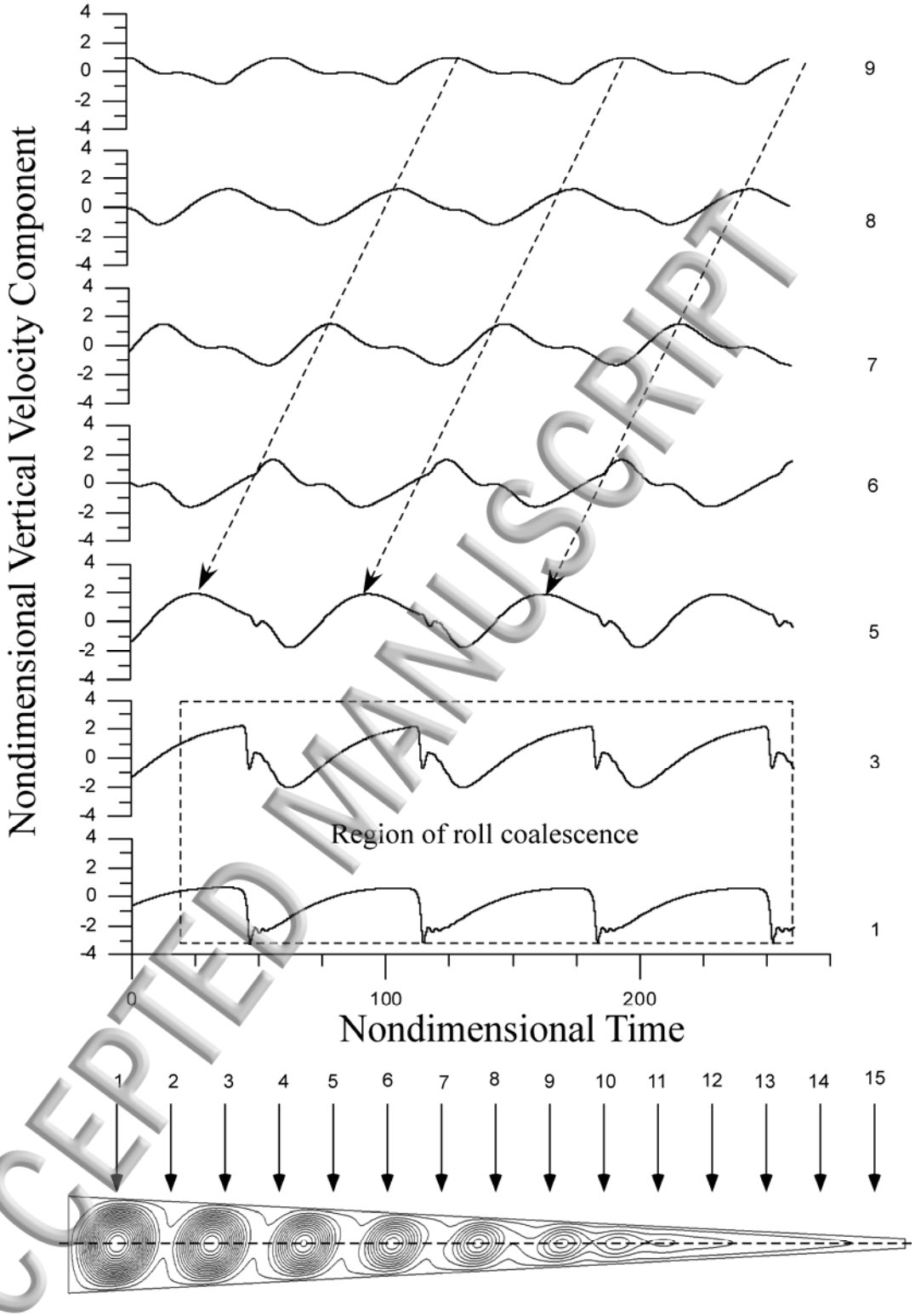

Fig. 14: Velocity signals provided by six probes equally spaced along the horizontal direction (A=20, η=0.1 and Ra=9000, vertical velocity component measured at y=0). The modulation of the sinusoidal signals being related to the main frequency is due to the presence of a second frequency in the spectrum for this relatively high value of the Rayleigh number (multimedia view available).

Some interesting analogies could be perhaps identified with a completely different phenomenon, typically occurring in high-Pr fluids subjected to thermally induced surface-tension gradients (namely, the so-called *hydrothermal waves* of Marangoni flow, Smith and Davis[50]; Shevtsova et al., [51]; Lappa[52-54]). Such waves, which also typically manifest as chain of travelling cells, however, do not display the local roll coalescence phenomena seen here. Moreover, their direction of propagation is univocally determined by the direction of the imposed temperature gradient (hydrothermal waves in Marangoni flow are known to propagate always in the same direction of the imposed temperature gradient, i.e. from the cold side to the hot side, whereas in the present case they can propagate in either directions depending on the value of η).

For A=10, we found the scenario for η=0.25 and η=4 to be very similar to that for η=0.1 and η=10, respectively, with the prevailing mode being essentially a wave travelling in the direction of increasing cross-sectional area (though the variation in η can exert some influence on the properties of the emerging solution, the fundamental mechanism does not change).

More specifically, we observed the increase in η from 0.1 to 0.25 to produce in some circumstances a higher number of coexisting rolls (m) participating to the wave mechanism (a variation from m=4 to m=5 for Ra=5000 and from m=5 to m=6 Ra=9000). For Ra=3000 and 7000, though a larger value of η does not change m, it can lead to a mitigation of the velocity of propagation of the rolls (as witnessed by the shrinkage visible in the related angular frequency). These trends can be also seen by taking a look at Fig. 11.

In the interest of conciseness, we do not discuss explicitly the results for η>1 as the aforementioned invariance principle relating to exchanging η with its reverse value (1/η) is still applicable. At this stage, however, we should clearly mention that though such a principle is valid for the velocity field, *it does not hold for the temperature field* (see again eq. (8)). This is witnessed by the change of direction of travelling waves with respect to the imposed temperature gradient when converging walls are replaced with diverging ones. In other words, for a fixed η, the problem *is not symmetric with respect to a change of the direction of the horizontally imposed temperature gradient* (namely the replacement of the hot and cold sidewalls). Another way to think about the thermal anisotropy intrinsically associated to this system is to consider that by keeping fixed the direction of the horizontal temperature gradient the problem would not be symmetric by replacing η with its reverse, i.e. 1/η. This anisotropy is typical of the Hadley flow, which being a shear flow (directed from the hot side to the cold side in proximity to the top wall and in the reversed sense near the bottom), breaks the isotropy of the considered system with respect to the x coordinate.

Continuing with our review of the numerical results, it is also worth examining in detail the case η=0.5 (η=2) for which we could notice some departure from the purely travelling disturbance seen for smaller (larger) values of η.

For relatively small values of the Rayleigh number (Ra=3000 and 5000) some limited differences can be noticed in the maximum of the streamfunction and in the angular frequency of the travelling wave for η=0.5 (η=2) and η=0.25 (η=4) (these quantities decrease as a function of η at fixed Ra for η<1, vice versa for η>1). Nevertheless, for relatively higher values of Ra (Ra≥7000) the most

This manuscript was accepted by Phys. Fluids. Click here to see the version of record.

notable feature distinguishing the patterns at η=0.25 and η=0.5 (η=4 and η=2) is the emergence of a *modulation locally affecting the flow in the right (left) part of the cavity*.

Surprisingly, starting from initially diffusive thermal conditions and using central differences, we found this (P) mode to become the dominant mechanism causing oscillations for η=0.5 (η=4) at Ra=7000 with the ensuing *suppression of the travelling disturbance*.

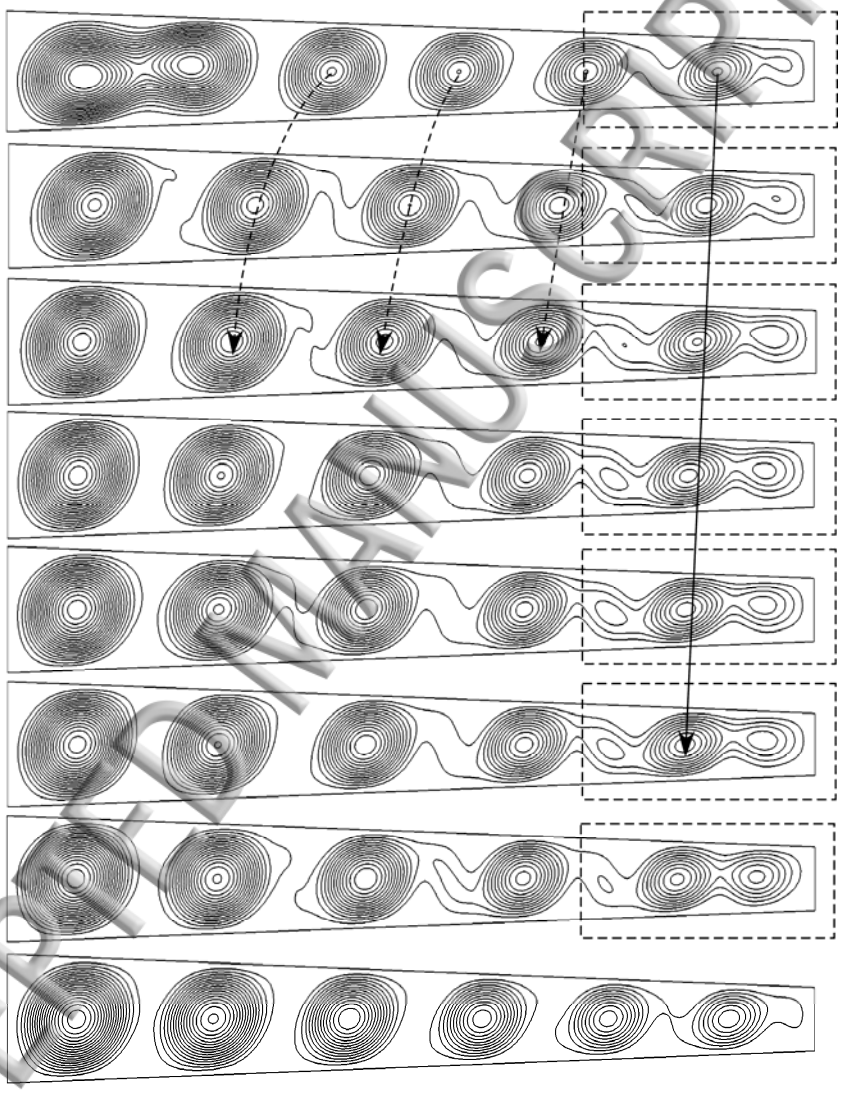

Fig. 15: Oscillatory convection for A=10, η=0.5 and Ra=9000: eight snapshots evenly distributed during one period of oscillation (multimedia view available).

In term of patterning behavior, such local effect manifests itself essentially via the formation of a three-roll structure periodically visible in the right part of the cavity (Fig. 15). This structure seems to be produced by the "splitting" of the original roll located near the right wall (this is why we have labeled this state as m="5+2"). As the reader will easily realize, most notably, this local sub-pattern

closely resembles the "twisted" recirculation embracing three co-rotating vortices that we have already discussed for the purely rectangular cavity with A=4 and Ra = 10^3 (Fig. 3a).

Because, we found the TW mechanism to re-enter the dynamics for Ra=9000, this led us again to the conclusion that for η=0.5 (η=2) multiple states of convection are possible (two in this case, namely, the TW or the P state) with one state being preferred to another according to the initial conditions and/or numerical scheme being used for the integration of the balance equations.

In order to verify once again the validity of the above statement, we repeated the simulation for η=0.5 and Ra=7000 by replacing central differences with the Van Leer scheme and obtained a purely travelling wave as for Ra=5000 and 9000.

Most interestingly, as for the case η=0.2 and A=4 discussed at the end of Sect. 3.1.1, for A=10 and η=0.5 we observed these two mechanisms to be both operative at Ra=9000 (Fig. 15, multimedia view), as witnessed by the two-frequency spectrum associated with this regime (it could be regarded as an example of what we have named (PLT) mode, namely a travelling wave "locally" modulated by roll pulsations or splitting behaviors). In particular, we found the typical timescale of the (P) mode to be smaller than the characteristic period of the TW (the characteristic frequency of the P disturbance is ω=1.319 whereas that of the wave it is approximately 0.05).

If η is finally increased (decreased) to 1, the above waveforms and related modulations effects are taken over by a completely different oscillations scenario where no clear direction of propagation of the disturbances can be identified. For such a specific case (rectangular enclosure), multiple states are known to exist in the form of configurations with different numbers of rolls. We have already discussed the typical properties of this regime in Sect. 3.1.1 and for this reason the related description is not duplicated here. We just limit ourselves to emphasizing once again the role played by the specific geometrical condition η=1 in separating regimes with *leftward* propagating waves from situations with *rightward* disturbance propagation. This should be regarded as a consequence of the intrinsic asymmetric nature of the Hadley flow (which being a shear flow *breaks the isotropy of the considered system with respect to reflections about the vertical coordinate*).

As a concluding remark for this section, towards the end to provide some additional insights into the influence of η on the threshold for the onset of time dependence, we finally discuss the specific dynamics seen for Ra=1000.

By moving along the horizontal direction for Ra=1000 in Fig. 10, indeed, the reader will immediately realize that an increase in η starting from η=0.1 (where the flow is steady with m=2) leads to flow destabilization with onset of oscillatory disturbances of the (K) type (still with m=2) for η=0.25 and a TW with m=3 for η=0.5. A further increase in η can revert the flow to steady conditions as witnessed by the solution obtained for η=1 (stationary flow with m=4).

The general destabilizing role played by η≠1 is also evident in Fig. 16 where the frequency has been reported as a function of η for fixed values of Ra. It can clearly be seen there that, while for η=1 the flow is steady for any value of Ra≤9000 (according to our simulations, for such a specific condition the Rayleigh number must be increased to 14500 in order to obtain oscillatory flow), for η=0.75 time-periodic convection is already possible for Ra=1000.

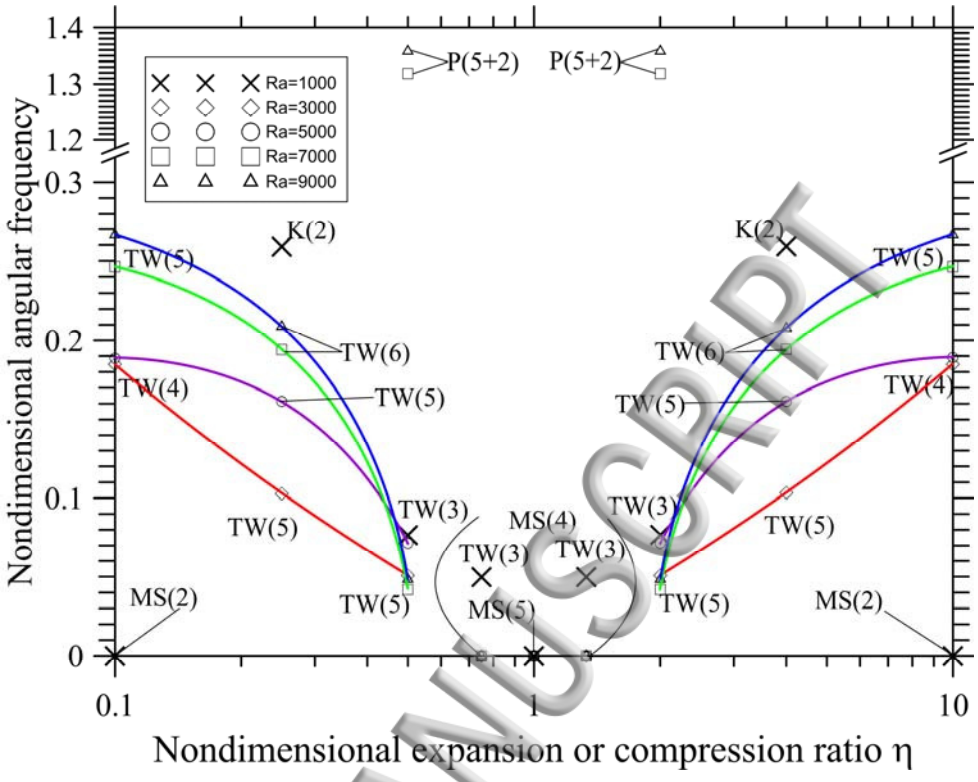

Fig. 16: Oscillatory angular frequency as a function of the expansion or compression rate η for A=10 and different values of the Rayleigh number (for η=1, the MS(5) flow becomes oscillatory for Ra>14000 with angular frequency ω≅6.48 for Ra=14500, not shown in the above plot).

Taken together, Figs. 10 and 16 also suggest that, though TW branches are dominant in the "external regions", the effective η intervals in which (TW) disturbances are possible at different values of the Rayleigh number shrink when Ra rises. This observation confirms the trends already discerned for A=4, i.e. that the preferential mechanism of oscillations is gradually transferred from low-frequency waves to high-frequency disturbances of the (P) type when Ra is increased.

4. Discussions and Conclusions:

Having completed a detailed description of the dynamics as a function of the aspect ratio, compression (or expansion) ratio η and Rayleigh number, we now turn to elaborating some general conclusions by filtering out specific details and concentrating on general trends.

To some extent such discussion is aimed to simplify the problem by abstracting from specific cases essential features. In doing so, in particular, we will heavily rely on the general maps shown in Figs. 4 and 10, by which a thorough analysis of the problem can be made more intuitive and manageable (as explained before, such maps are essentially diagrams with η as abscissa and Ra as ordinate where the results provided by the numerical simulations have been collected in an ordered fashion).

This manuscript was accepted by Phys. Fluids. Click here to see the version of record.

In the following, in particular, we start from an analysis of the wavenumber, namely the number of rolls simultaneously present in the enclosure.

From a purely theoretical standpoint, it is known that, in general, the spacing of the cells pertaining to the 2D hydrodynamic mode can be assumed to depend on a number of factors. First is the fact that an integral number of cells must be accommodated into a cavity of finite extension and the inter-roll distance must satisfy this constraint. The second factor is the magnitude of the departure from the onset of instability. Third is the obvious role played by converging or diverging boundaries in constraining the flow in the end regions and how this effect changes with the Rayleigh number.

The influence of the aspect ratio can be immediately clarified by cross-comparison of the results for A=4 and A=10 from which it becomes evident than an increase in A significantly expands the set of wavenumbers allowed in the system (this ranging from 1 to 5+2 for A=10 and from 1 to 3 only for A=4 over the considered interval of Ra). Such a dependence, however, is not as straightforward as one would imagine because it *is mediated by the influence of the expansion (or compression) ratio* η, especially for A=10.

For such a value of A, we found an increase (a decrease) in η from the condition $\eta \cong 1$ to determine a shrinkage in the number of rolls, whereas an increase in the Rayleigh number is generally responsible for higher values of the wavenumber m, the angular frequency and an increase in the complexity of the frequency spectrum (with the possible coexistence in some circumstances of disturbances operating at different time and spatial scales).

The most interesting information provided by these maps, however, is the evidence they give in terms of transition from one regime to another. Indeed, it is possible to clearly discern three distinct regions of spatio-temporal behavior. The central one is the region of "standard" hydrodynamic modes emergence, that is the area of the space of parameters (η, Ra) where the Hadley flow is affected by the typical "pulsating" disturbances (P) already revealed in past studies for the case of perfectly rectangular cavities. The two external regions, however, are the loci of heretofore unseen dynamics. The typical pulsating disturbance can be taken over in such intervals by a completely new mechanism by which the disturbance is seen to spread continuously along the horizontal direction giving rise to "travelling waves".

While for A=4 such phenomena can be barely seen because of the coexistence with (K)-modes at intermediate values of η, or they are hardly recognizable because of the simultaneous occurrence of roll coalescence processes (which overshadow or mask the continuous propagation of the disturbance), for A=10 they become the preferred mode of oscillatory instability over a wide range of η. Moreover such a value of the aspect ratio is sufficiently large to allow the observer to filter out other localized phenomena (such as the roll coalescence process taking place in proximity to the walls).

Another conclusion stemming from all these observations is that for relatively large aspect ratios, two main categories of disturbances affecting the considered dynamics can be identified in terms of frequency, namely, a small-frequency large-scale disturbance (manifesting itself in space as a TW),

and a high-frequency small-scale disturbance (corresponding essentially to localized pulsating phenomena or kissing rolls). The preceding discussion, however, should not be misread as implying that these modes follow a precise trajectory in the space of parameters. Though, for relatively small values of Ra, the two disturbances manifest separately, they are not mutually exclusive, nor are they truly progressive. As revealed by the present approach based on extensive parametric simulations (assuming different initial conditions and/or integration schemes for fixed cases), these modes correspond to the existence of "multiple" states of convection. In some cases (essentially in the high-Ra part of the space of parameters), modes pertaining to different branches can coexist leading to states in which a low-frequency (traveling) disturbance is modulated locally by a high-frequency (pulsating) perturbation.

References

[1] Delgado-Buscalioni R. and Crespo del Arco E., (2001), Flow and heat transfer regimes in inclined differentially heated cavities, *Int. J. Heat Mass Transfer*, 44: 1947-1962.
[2] Kaddeche S., Henry D. and Ben Hadid H., (2003), Magnetic stabilization of the buoyant convection between infinite horizontal walls with a horizontal temperature gradient, *J. Fluid Mech.,* 480 (2003): 185-216.
[3] Li Y.R., Peng L., Wu S.-Y., Imaishi N., Zeng D.L., (2004), Thermocapillary-buoyancy flow of silicon melt in a shallow annular pool, *Cryst. Res. Tech*, 39(12): 1055-1062.
[4] Okano Y., Itoh M. and Hirata A., (1989), Natural and Marangoni Convections in a Two-Dimensional Rectangular Open Boat, *Journal of Chemical Engineering*, 22(3): 275-281.
[5] Jaber T.J. and Saghir M.Z., (2006), The Effect of Rotating Magnetic Fields on the Growth of SiGe Using the Traveling Solvent Method, *Fluid Dyn. Mater. Process*., 2(3): 175-190.
[6] Lappa M., (2007), Secondary and oscillatory gravitational instabilities in canonical three-dimensional models of crystal growth from the melt, Part2: Lateral heating and the Hadley circulation, *Comptes Rendus Mécanique*, 335(5-6): 261-268.
[7] Lappa M., (2017), On the oscillatory hydrodynamic modes in liquid metal layers with an obstruction located on the bottom, *Int. J. Thermal Science*, 118: 303–319.
[8] Ludwig A., Gruber-Pretzler M., Wu M., Kuhn A. and Riedle J., (2005), About the Formation of Macrosegregations During Continuous Casting of Sn-Bronze, *Fluid Dyn. Mater. Process*., 1(4) (2005): 285-300.
[9] Abhilash E., Joseph M.A. and Krishna P., (2006), Prediction of Dendritic Parameters and Macro Hardness Variation in Permanent Mould Casting of Al-12%Si Alloys Using Artificial Neural Networks, *Fluid Dyn. Mater. Process*., 2(3): 211-220.
[10] Dupret F. and Van der Bogaert N., Modelling Bridgman and Czochralski growth, in Handbook of Crystal Growth (ed. D. T. J. Hurle) 2: 877-1010. North-Holland, Amsterdam (1994).
[11] Monberg E., "Bridgman and related growth techniques". In Handbook of Crystal Growth (ed. D. T. J. Hurle), 2: 53-97. North-Holland, Amsterdam (1994).
[12] Zrodnikov A.V., Efanov A.D., Orlov Yu.I., Martinov P.N., Troynov V.M., Rusanov A.E., (2004), Technology of heavy liquid metal coolants lead-bismuth and lead, VANT, Serial: Provision of NPP Safety, Issue 4, Nuclear Technologies for Future Power System, (2004): 180–184.
[13] Luo M. and Liu J., (2013), Experimental investigation of liquid metal alloy based mini-channel heat exchanger for high power electronic devices, *Frontiers in Energy*, 7(4):479-486. DOI: 10.1007/s11708-013-0277-3
[14] Lappa M., Thermal Convection: Patterns, Evolution and Stability, John Wiley & Sons, Ltd (2009, Chichester, England).

[15] Ostroumov G.A. (1952), *Free convention under the conditions of the internal problem*, NACA TM, Washington, April 1958, Translation of *Svobodnaya convectzia v ousloviakh vnoutrennei zadachi*, State Publishing House, Technico-Theoretical Literature, Moscow-Leningrad, 1952.
[16] Birikh R.V., (1966), Thermocapillary convection in a horizontal fluid layer, *J. Appl. Mech. Tech. Phys*. **7**: 43-49.
[17] Lappa M., (2012), Exact Solutions for Thermal Problems: Buoyancy, Marangoni, Vibrational and Magnetic-Field-Controlled Flows, *Review of Applied Physics*, 1(1): 1-14.
[18] Adomian G., (1990), A review of the decomposition method and some recent results for nonlinear equations, *Math. and Comp. Mod*., 13: 17-43.
[19] Cherruault Y. and Adomian G., (1993), Decompositon method, A new proof of convergence, *Math. and Comp. Mod*. 18: 103-106.
[20] Babolian E., Vahidi A.R., Asadi Cordshooli G.H., (2005), Solving differential equations by decomposition method, *Appl. Math. Comput*. 167: 1150-1155.
[21] Makinde O. D., (1997), Steady flow in a linearly diverging asymmetrical channel, *CAMES*, 4: 157-165.
[22] Mhone P. Y. and Makinde O. D., (2006), Unsteady MHD flow with heat transfer in a diverging channel, *Romanian J. Phys*., 51 : 963-975.
[23] Asadullah, M., Khan, U., Manzoor, R., Ahmed, N., & Mohyud-Din, S. T. (2013), MHD flow of a Jeffery fluid in converging and diverging channels. *Int. J. Mod. Math*. Sci, 6(2), 92-106.
[24] Lappa M. and Ferialdi H., (2017), On the General Properties of Steady Gravitational Thermal Flows of Liquid Metals in Variable Cross-section Containers, *Review of Applied Physics* (ISSN: 2327-1604), 5(1): 1-10. DOI: 10.14355/rap.2017.05.001
[25] Hadley G., (1735), Concerning the cause of the general trade winds, *Phil. Trans. Roy. Soc. Lond.*, 29: 58-62.
[26] Tollmien W., (1936), General instability criterion of laminar velocity distributions, Tech. Memor. Nat. Adv. Comm. Aero., Wash. No. 792 (1936).
[27] Lin C.-C., (1944), On the stability of two-dimensional parallel flows, *Proc. NAS*, 30(10) (1944): 316-324.
[28] Rosenbluth M.N. and Simon A., (1964), Necessary and sufficient conditions for the stability of plane parallel inviscid flow, *Phys. Fluids*, 7(4) (1964): 557-558.
[29] Drazin P. and Howard L.N., (1966), Hydrodynamic stability of parallel flow of inviscid fluid, *Adv. Appl. Mech.*, 9: 1-89.
[30] Hurle D.T.J., (1966), Temperature oscillations in molten metals and their relationship to growth striae in melt-grown crystals, *Phil. Mag*., 13: 305-310.
[31] Hart J.E., (1972), Stability of thin non-rotating Hadley circulations,. *J. Atmos. Sci*., 29: 687-697.
[32] Hart J.E., (1983), A note on the stability of low-Prandtl-number Hadley circulations, *J. Fluid Mech*., 132: 271-281.
[33] Gill A. E., (1974), A theory of thermal oscillations in liquid metals, *J. Fluid Mech.* 64 (3): 577-588.
[34] Laure P. and Roux B., (1989), Linear and non linear study of the Hadley circulation in the case of infinite cavity, *J. Cryst. Growth* 97(1): 226-234.
[35] Kuo, H. P. and Korpela, S. A. (1988) Stability and finite amplitude natural convection in a shallow cavity with insulated top and bottom and heated from the side, *Phys. Fluids*, 31, 33–42.
[36] Wang T.-M. and Korpela S.A., (1989), Longitudinal Rolls in a Shallow Cavity Heated from a Side, *Phys. Fluids* A, 32: 947-953.
[37] Crespo del Arco E., Pulicani P. P. and Randriamampianina A., (1989), Complex multiple solutions and hysteresis cycles near the onset of oscillatory convection in a Pr = 0 liquid submitted to a horizontal temperature gradient, *C. R. Acad. Sci. Paris* 309, II, 1869-1876.

[38] Pulicani J. P., Del Arco E. C., Randriamampianina A., Bontoux P., and Peyret R., (1990), Spectral simulations of oscillatory convection at low Prandtl number. *International Journal for Numerical Methods in Fluids*, 10(5), 481-517.
[39] Okada K., and Ozoe H., (1993), Various computational conditions of oscillatory natural convection of zero Prandtl number fluid in an open boat heated and cooled from opposing vertical walls, *Numerical Heat Transfer*, Part A Applications, 23(2), 171-187.
[40] Okada K. and Ozoe H., (1993), The Effect of Aspect ratio on The critical Grashof number for Oscillatory Natural Convection of Zero Prandtl Number Fluid: Numerical Approach, *J. Cryst. Growth*, 126: 330-334.
[41] Gelfgat A.Yu., Bar-Yoseph P.Z. and Yarin A.L., (1997), On Oscillatory instability of Convective Flows at Low Prandtl Number, *Journal of Fluids Engineering*, 119: 823-830.
[42] Gelfgat A.Yu., Bar-Yoseph P.Z. and Yarin A.L., Stability of Multiple Steady States of Convection in Laterally Heated Cavities, *J. Fluid Mech.*, 388 (1999): 315-334.
[43] Jang D.S., Jetli R., Acharya S. (1986), Comparison of the PISO, SIMPLER and SIMPLEC algorithms for the treatment of the pressure-velocity coupling in steady flow problems. *Numer Heat Transfer* 10: 209–228.
[44] Moukalled F., Mangani L. and Darwish M., (2016), The Finite Volume Method in Computational Fluid Dynamics - An Advanced Introduction with OpenFOAM and Matlab, Springer International Publishing, 2016, New York).
[45] Choi SK, Nam HY, Cho M (1994) Systematic comparison of finite-volume calculation methods with staggered and nonstaggered grid arrangements. *Numer Heat Transfer, Part B* 25 (2): 205–221
[46] Choi SK, Nam HY, Cho M (1994a) Use of staggered and nonstaggered grid arrangements for incompressible flow calculations on nonorthogonal grids. *Numer Heat Transfer, Part B* 25(2): 193–204.
[47] Rhie C.M. and Chow W.L., (1983), Numerical study of the turbulent flow past an airfoil with trailing edge separation. *AIAA J* 21:1525–1532
[48] Patankar S.V. and Spalding D.B., (1972), A calculation procedure for heat, mass and momentum transfer in three-dimensional parabolic flows, *Int. J. Heat Mass Transfer*, 15:1787-1806.
[49] Van Doormaal J.P. and Raithby G.D. (1985), An evaluation of the segregated approach for predicting incompressible fluid flows, In National Heat Transfer Conference, Denver, Colorado, August 4-7, 1985.
[50] Smith M.K., Davis S.H. (1983), Instabilities of dynamic thermocapillary liquid layers. Part 1 : convective instabilities, *J. Fluid Mech* 132: 119-144.
[51] Shevtsova V.M., Nepomnyashchy A.A. and Legros J.C., (2003), Thermocapillary-buoyancy convection in a shallow cavity heated from the side, *Phys. Rev. E 67*, 066308 (14 pages)
[52] Lappa M., (2016), Patterning behavior of gravitationally modulated supercritical Marangoni flow in liquid layers, *Phys. Rev. E*, 93(5), 053107, (13 pages).
[53] Lappa M., (2017), Hydrothermal waves in two-dimensional liquid layers with sudden changes in the available cross-section, *Int. J. Num. Meth. Heat Fluid Flow* (ISSN: 0961-5539), Accepted, DOI: 10.1108/HFF-11-2016-0453
[54] Lappa M., (2016), On the onset of multi-wave patterns in laterally heated floating zones for slightly supercritical conditions, *Phys. Fluids*, 28(12): 124105 (22 pages).